Chemical Science

EDGE ARTICLE

View Article Online
View Journal | View Issue

Cite this: *Chem. Sci.*, 2014, **5**, 1368

Solid-state structural transformation doubly triggered by reaction temperature and time in 3D metal-organic frameworks: great enhancement of stability and gas adsorption†

Ping Shen,[a] Wen-Wen He,[a] Dong-Ying Du,[a] Hai-Long Jiang,[c] Shun-Li Li,[b] Zhong-Ling Lang,[a] Zhong-Min Su,*[a] Qiang Fu[a] and Ya-Qian Lan*[ab]

Received 24th September 2013
Accepted 2nd December 2013

DOI: 10.1039/c3sc52666f

www.rsc.org/chemicalscience

In this work, we have demonstrated an unprecedented single-crystal-to-single-crystal (SCSC) transformation between two 3D metal-organic frameworks (MOFs). The centrosymmetric **IFMC-68** ($[(Zn_4O)_2(L)_3]\cdot 10H_2O\cdot 46DMA$) transforms into a chiral **IFMC-69** ($[(Zn_4O)_2(L)_3H_2O]\cdot H_2O\cdot 4DMA$) doubly triggered by reaction temperature and time simultaneously in the presence or absence of solvent. To our knowledge, this is the first representative that the non-interpenetrated structure transforms into self-penetrated structure in MOFs. For the first time, we have studied the influence of reaction temperature and time on SCSC transformation, simultaneously, and get the transformation relationship among **IFMC-68**, **IFMC-69** and the intermediate coming from the direct synthesis method and stepwise synthesis method at different temperatures and for different times. Meanwhile, we have achieved the conversion from an air-unstable to air-stable structure. Air-stable **IFMC-69** exhibits the selective CO_2 uptake over N_2 and more excellent gas adsorption ability than **IFMC-68**. In addition, **IFMC-69** shows an efficient capability in reversible adsorption of iodine. The electrical conductivity value (σ) of I_2**@IFMC-69** is much higher than the pristine MOF and thus is promising for potential semiconductor materials in the future.

Introduction

Single-crystal-to-single-crystal (SCSC) structural transformations, which involve cooperative movements of atoms in the solid state, are very fascinating and one of the hot topics in solid-state chemistry.[1] The first report of SCSC transformations was a photoreaction in organic complexes,[2] and then the SCSC transformations were extended to other complexes.[3] In the past decades, the studies of SCSC structural transformation in metal-organic frameworks (MOFs) have been met with great interest and have developed rapidly, because it allows direct visualization of how the crystal structure is changing during the transformation process.[4] Most of these reports are the transformations caused by sliding of layers or the breathing of 3D porous MOFs through guest removal or solvent exchange.[5] The SCSC transformations caused by photochemical [2 + 2] cycloadditions generating new organic molecules have been well studied in coordination polymers (or MOFs).[6] However, the SCSC transformations including the cleavage and regeneration of coordination bonds remain less common.[7] In particular, the SCSC transformations between 3D structures are still quite rare, because it is difficult for 3D MOFs to retain their crystallinity after breaking and forming coordination bonds in the solid phase.[8] Hitherto, only limited examples of 3D → 3D SCSC transformations have been observed by the groups of Kim, zur Loye and Chen.[9] Therefore, studying the SCSC transformation resulting from the cleavage and regeneration of coordination bonds between 3D structures is one of the most challenging issues in synthetic chemistry and solid-state chemistry.

Almost all MOF materials that have been published thus far are synthesized in a solvothermal black box using the concepts of zeolite chemistry. The reaction process is so mysterious that it prompts us to investigate what on earth happened in it, especially for the crystals synthesis process of SCSC transformation in the solid state. SCSC transformation can be triggered by external stimuli, such as light, heat, guest removal, uptake or exchange, expansion of coordination numbers, oxidation of metal centers, or reactions between the ligands.[10] In previous reports on SCSC transformation reactions caused by

[a]*Institute of Functional Material Chemistry, Faculty of Chemistry, Northeast Normal University, Changchun 130024, P.R. China. E-mail: zmsu@nenu.edu.cn*

[b]*Jiangsu Key Laboratory of Biofunctional Materials, College of Chemistry and Materials Science, Nanjing Normal University, Nanjing 210023, P.R. China. E-mail: yqlan@njnu.edu.cn*

[c]*Hefei National Laboratory for Physical Sciences at the Microscale, Department of Chemistry, University of Science and Technology of China, Hefei 230026, P.R. China*

† Electronic supplementary information (ESI) available: Full experimental details, figures, tables and crystallographic data in CIF format. CCDC 935302 and 922086. For ESI and crystallographic data in CIF or other electronic format see DOI: 10.1039/c3sc52666f

heat, chemists have taken into consideration the temperature influences on the reaction.[1c,11] However, SCSC transformation studies involving both the reaction temperature and time are rarely reported, and may help us understand whether the formation process of crystals *via* SCSC transformation is kinetically or thermodynamically controlled. It is a challenge to find a suitable system to investigate the influence of both reaction temperature and time on the SCSC transformation simultaneously.

Herein, we report an unprecedented SCSC transformation system between two 3D MOFs. The centrosymmetric **IFMC-68** ($[(Zn_4O)_2(L)_3]\cdot 10H_2O\cdot 46DMA$) (**IFMC** corresponds to Institute of Functional Material Chemistry) transforms into chiral **IFMC-69** ($[(Zn_4O)_2(\mathbf{L})_3H_2O]\cdot H_2O\cdot 4DMA$) doubly triggered by reaction temperature and time simultaneously in solvent and solid state, where H_4L is methanetetra(tetrakis[4-(carboxyphenyl)oxamethyl]-methane acid). To our knowledge, there are no examples of SCSC transformations between 3D structures *via* the dimerization of $Zn_4O(CO_2)_6$ clusters by one H_2O molecule. More importantly, we have achieved the conversion from an air-unstable structure to an air-stable one. Meanwhile, it is the first representative that the non-interpenetrated structure transforms into self-penetrated structure in MOFs. Air-stable **IFMC-69** exhibits the more excellent gas adsorption ability than **IFMC-68**. In addition, **IFMC-69** shows an efficient capability in reversible adsorption of iodine, and the electrical conductivity value (σ) for **I_2@IFMC-69** is 2.80×10^{-6} S cm^{-1}, which is obviously higher than that of **IFMC-69** (1.25×10^{-13} S cm^{-1}).‡

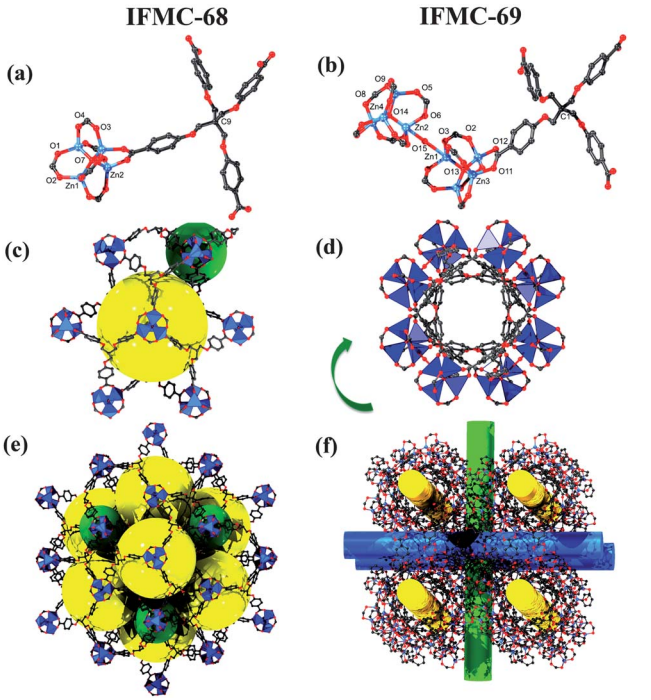

Fig. 1 (a) and (b) show the coordination environments of $Zn_4O(CO_2)_6$ SBU in **IFMC-68** and $[Zn_4O(CO_2)_6]_2H_2O$ SBU in **IFMC-69**, respectively. (c) Two types of cages in **IFMC-68**. (d) Representation of the 1D channel in **IFMC-69**. (e) View of the 3D network of **IFMC-68** along the *c*-axis. (f) The channel and ball-and-stick representation of the three directional channels in **IFMC-69**. All hydrogen atoms have been omitted for clarity. Blue = Zn; dark gray = C; red = O.

Results and discussion

A single-crystal X-ray diffraction study reveals that **IFMC-68** crystallizes in the trigonal space group $R\bar{3}c$. The asymmetric unit (Fig. 1a) contains one Zn_4O cluster consisting of four Zn cations, one μ_4-O atom, and one L^{4-} ligand. The tetrahedral Zn_4O cluster is encapsulated by six carboxylate groups from different L^{4-} to form a classic $Zn_4O(CO_2)_6$ secondary building unit (SBU). The overall structure of **IFMC-68** is a 3D (4,6)-connected network (Fig. S1†) with ideal corundum structure, in which the L^{4-} is regarded as a four-connected node and the $Zn_4O(CO_2)_6$ SBU is regarded as a six-connected node. The resultant non-interpenetrated **IFMC-68** features a quadrangular opening, and two types of microporous and mesoporous cages (Fig. 1c). With such an assembly, each microporous cage is surrounded by eight mesoporous cages, which results in very high free porosities of 80% in **IFMC-68** (Fig. 1e). The structure of **IFMC-68** is isomorphic to the mesoporous MOFs in Lan and Xu's paper,[13] and the cage-based MOF has been reported by the Cao group.[14]

IFMC-69 crystallizes in the chiral space group of *P*23. The asymmetric unit (Fig. 1b) contains four kinds of Zn ions, two kinds of μ_4-O atoms, one L^{4-} ligand and one coordination water molecule. Zn1 and Zn2 are five-coordinated trigonal bipyramidal geometries, which are surrounded by three carboxylic oxygen atoms from different ligands, one μ_4-O atom and one water molecule. Zn3 and Zn4 show tetrahedral coordinated geometries which are formed by three carboxylic oxygen atoms from different ligands and one μ_4-O atom. Different from the structure of **IFMC-68**, there are two $Zn_4O(CO_2)_6$ clusters in **IFMC-69**. These two $Zn_4O(CO_2)_6$ clusters are connected by one water molecule to generate a new $[Zn_4O(CO_2)_6]_2H_2O$ SBU. To the best of our knowledge, it represents the first example that the classic $Zn_4O(CO_2)_6$ SBU connected by water to form a new $[Zn_4O(CO_2)_6]_2H_2O$ SBU. One Zn_4O cluster is coordinated by six ligands and one water molecule, which can be regarded as a 7-connected node, and each L^{4-} ligand is bonded to four Zn_4O clusters (two kinds of clusters), acting as a 4-connected node. Therefore, the overall 3D framework can be regarded as a (4,7)-connected net (Fig. S2†), which has not been reported yet. In the (4,7)-connected topology, two kinds of rings (in red and green) interpenetrate with each other, and a linker (in purple) connects the two kinds of rings to form a self-penetrated structure of **IFMC-69** (Fig. S3†). If regarding the $[Zn_4O(CO_2)_6]_2H_2O$ SBU, which is connected by twelve ligands, as a 12-connected node and each L^{4-} ligand as a 4-connected node, the 3D framework is going to be a (4,12)-connected topology (Fig. S4†). A more interesting feature in this resultant MOF is that there are interweaved channels along the three directions (Fig. 1f), the diameter of which is 6.46 Å (Fig. 1d and S8†). The calculated free volume in fully desolvated **IFMC-69** is 37.9% by PLATON.[12]

Then we perform the further study into the nature of these intricate architectures. When taking no account of the

coordination water molecule in the $[Zn_4O(CO_2)_6]_2H_2O$ SBU (Fig. S5c†), one Zn_4O cluster is coordinated by six ligands to be a 6-connected node and each tetratopic ligand is bonded to four Zn_4O clusters (two kinds of clusters) to be a 4-connected node, and this results in a (4,6)-connected 3D MOF (Fig. S5d and S7b†). The whole structure is composed of three parts. Two of them are separated 2-fold units which can coincide with each other by a rotation of 45° in the plane. Additionally, these two units connect with each other by sharing the third part consisting of ligands (shown in black in Fig. S5g†) to form a complicated 3D structure with self-penetrated character (Fig. S5c, S5e and S6†).

IFMC-68 was synthesized *via* solvothermal reactions of semi-rigid carboxylate linker H_4L, $Zn(NO_3)_2\cdot 6H_2O$ and 5 mL DMA or DMF at 85 °C for 72 h. For **IFMC-69**, the other synthetic condition is similar to that for **IFMC-68** only by increasing the temperature to 140 °C. Owing to the similarity and the continuity of the synthesis process of these two crystals, we discuss the products obtained at 140 °C for different time. Powder X-ray diffraction (PXRD) data (Fig. 2) shows the products are pure **IFMC-68** heated at 140 °C for 24 h. After 48 h, PXRD of the products shows that they are the intermediates including **IFMC-68** and **IFMC-69**, and the small single crystals in the intermediate are determined as **IFMC-69** by X-ray single-crystal diffraction. More importantly, we obtain the photos of the intermediates, which provide more direct evidence for the existence of intermediates (Fig. 2). The single crystal in red circle is determined as **IFMC-69** by X-ray single-crystal diffraction, and the remaining part is **IFMC-68**. After 72 h, **IFMC-69** has been completely obtained based on the original reactant H_4L and $Zn(NO_3)_2\cdot 6H_2O$. These investigation results demonstrate **IFMC-68** is a precursor in the formation process of **IFMC-69** in direct synthesis method. There may be a SCSC transformation from **IFMC-68** to **IFMC-69** during the process.

Hence, we assume that **IFMC-69** may be obtained by using the step-wise method. The as-synthesized **IFMC-68** (50 mg) was put into a Teflon liner with 5 mL DMA and heated at 140 °C for 72 h. As expected, **IFMC-69** is successfully obtained from the precursor of **IFMC-68**, and it may be a SCSC transformation. Experiments were performed following the reported method to explore whether the transformation from **IFMC-68** to **IFMC-69** belongs to a solid to solid mechanism or a dissolution and re-crystallization mechanism.[15] One crystal of **IFMC-68** was selected and inserted into a 0.8 mm diameter melting point tube 0.3 mL DMA (Fig. 3a), and then was heated at 140 °C for 72 h. The outline of the gathered crystals remained the same as **IFMC-68**. When pressed lightly, we got the dispersive little single crystals of **IFMC-69** which can be confirmed by X-ray single-crystal analysis (Fig. 3b). The photographs taken under the optical microscope prove that there is no dissolving or re-crystallizing of any crystals, so it is a real SCSC transformation (Fig. 3). The PXRD results show that the SCSC transformation from **IFMC-68** to **IFMC-69** can be successfully achieved in DMF or DMA, but failed in ethanol or methanol (Fig. S9†).

We try to achieve this SCSC transformation in solid-state without any solvent. The single crystal of **IFMC-68** was selected and sealed in a 0.8 mm diameter melting point tube without solvent (Fig. 3c), and then it was heated at 140 °C for 72 h. The result of this solid transformation was similar to the solvent transformation described above, except the crystallization of **IFMC-69** changed a little, meanwhile the cubic **IFMC-68** transformed to smaller irregular shape microcrystalline of **IFMC-69** (Fig. 3d). PXRD results indicate that the as-synthesized samples match the simulated pattern of **IFMC-69** very well (Fig. S10†). The aforementioned transformation process can be also achieved in a sealed Teflon liner, and it proves that the solid-state SCSC transformation from **IFMC-68** to **IFMC-69** can be realized by thermal method without any solvent.

Furthermore, we discussed the reaction conditions of the SCSC transformation from **IFMC-68** to **IFMC-69**. Firstly, **IFMC-68** was heated at different temperatures ranging from 85 °C to 160 °C for 72 h in Teflon reactor without solvent, and the PXRD

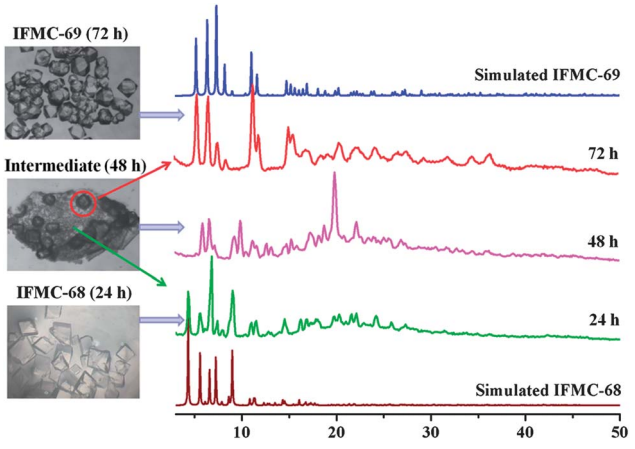

Fig. 2 Powder X-ray diffraction patterns of simulated **IFMC-68** (dark red), the products from direct synthesis method at 140 °C for 24 h (green), 48 h (pink), 72 h (red) and simulated **IFMC-69** (blue). Photos of crystals (left) after heating to 140 °C for 24 h, 48 h and 72 h, respectively.

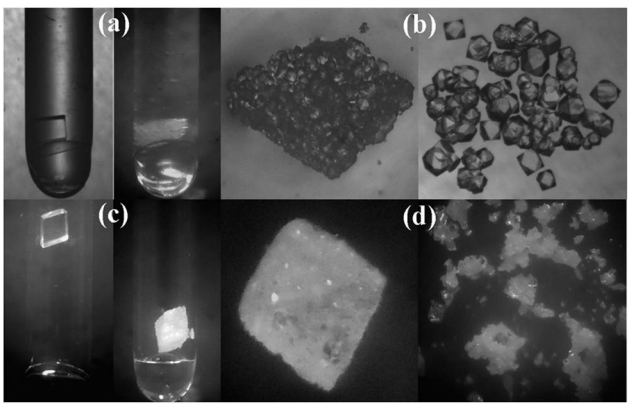

Fig. 3 Photographs of the SCSC transformation from **IFMC-68** to **IFMC-69**. Photos of single crystal of **IFMC-68** sealed in a melting point tube before (left) and after (right) heating at 140 °C for 72 h in 0.3 mL DMA (a), and without solvent (c), respectively. Enlarged photos of crystals sealed in a melting point tube and dispersive crystals heating at 140 °C for 72 h in DMA (b), and without solvent (d), respectively.

patterns reveal that the SCSC transformation can take place from 140 °C to 160 °C (Fig. S10†). Then 140 °C was selected as a representative temperature to investigate the SCSC transformation in solid state. We also try to monitor the SCSC transformation by variable-temperature (VT)-PXRD of **IFMC-68** under air, but the results show **IFMC-68** can not transform into **IFMC-69** (Fig. S11†). This may be because the testing time is so short that the transformation does not have enough time to complete. Keeping this in mind, we supposed that the reaction time may be another important factor during the SCSC transformation. Then the influence of the reaction time has been studied. When **IFMC-68** is heated at 140 °C without solvent for 6 h, it is still **IFMC-68**; the product is intermediate for 12–21 h; after 24 h until up to 72 h, **IFMC-69** is obtained completely. The SCSC transformation without solvent can also be detected by PXRD patterns (Fig. 4). As shown in the shadow parts, the diffraction intensity corresponding to (1, 0, $\bar{2}$) and (1, 0, $\bar{8}$) crystallographic planes at 4.31° (peak 1) and 8.98° (peak 2), respectively, in 2θ of **IFMC-68** gradually decrease from 6 h to 24 h, and new peak corresponding to (3, 0, 0) crystallographic plane at 11.07° (peak 3) in 2θ of **IFMC-69** starts to appear more prominently from 6 h to 24 h. From 12 h to 21 h, the profile of the PXRD patterns does not show any evidence of **IFMC-68** upon further time to 24 h, indicating completion of the transformation into **IFMC-69**. In summary, **IFMC-68** can transform to **IFMC-69** at 140 °C without solvent after 24 h.

IFMC-69 can be obtained by direct synthesis and step-wise synthesis methods. In order to further understand the mechanism of the SCSC transformation and explore the influence of reaction time and temperature on the products, similar experiments based on different temperatures and time have been performed. The transformation relationship between **IFMC-68** and **IFMC-69** is in Scheme 1, and the experimental data are listed in Table S1.† According to the data, selecting time and temperature as *X* and *Y*-axis, we get the transformation relationship diagrams of **IFMC-68**, **IFMC-69** and the intermediate coming from the direct synthesis method and stepwise synthesis methods. For the direct synthesis method in DMA or DMF (Fig. S12†), when heated at 140 °C for 24 h or 130 °C for 36 h or 120 °C for 48–72 h, the product is **IFMC-68**; when heated at 160 °C for 24–48 h or 150 °C for 36 h or 140 °C for 72 h, **IFMC-69** is attained. The area between **IFMC-68** and **IFMC-69** represents the synthesis condition for the intermediate. Similarly, for the step-wise synthesis method (**IFMC-68**) in DMA or DMF (Fig. S13†) and without solvent (Fig. S14†), the areas between **IFMC-68** and **IFMC-69** represent the synthesis condition for the intermediate, respectively. To sum up, the SCSC transformations between **IFMC-68** and **IFMC-69** are triggered by reaction temperature and time simultaneously in either solvent or solid state. When 50 mg **IFMC-69** was sealed in a Teflon liner with 5 mL DMA and heated at 85, 100, 120 or 140 °C for 72 h, **IFMC-69** still remained. **IFMC-69** cannot turn to **IFMC-68** in solvent under lower temperature. Therefore, the SCSC transformation is irreversible.

According to the phenomenon occurring in the SCSC transformation, we suppose the solvent molecules move faster in channels with heating, which results in the partial coordination bonds of unstable **IFMC-68** breaking. Then different $Zn_4O(CO_2)_6$ SBUs move closer to each other and coordinate with the water molecules to form new $[Zn_4O(CO_2)_6]_2H_2O$ SBUs which recombine to generate the new compound (**IFMC-69**) in certain time. **IFMC-68** is a kinetic product, formed easily from the components at relatively low temperature. With the increasing the time and temperature, this unstable product progressively converts into the thermodynamic product of **IFMC-69**. During the SCSC transformation process, the transformation from the $Zn_4O(CO_2)_6$ SBU to the $[Zn_4O(CO_2)_6]_2H_2O$ SBU is very crucial. In order to confirm this prediction, quantum chemical calculations have been performed to simulate the reaction on the basis of density functional theory method (DFT) by selecting $Zn_4O(CO_2)_6$ SBU and $[Zn_4O(CO_2)_6]_2H_2O$ SBU as simple models, with the benzenes substituted by H atoms (Fig. S15†). All calculations are performed at PCM/B3LYP/[LANL2DZ(Zn)/6-31 + g*(O, H, C)] level with Gaussian 09 software package. According to the experimental conditions reported above, the formation of **IFMC-69** is carried out at 140 °C. Thus the calculation condition

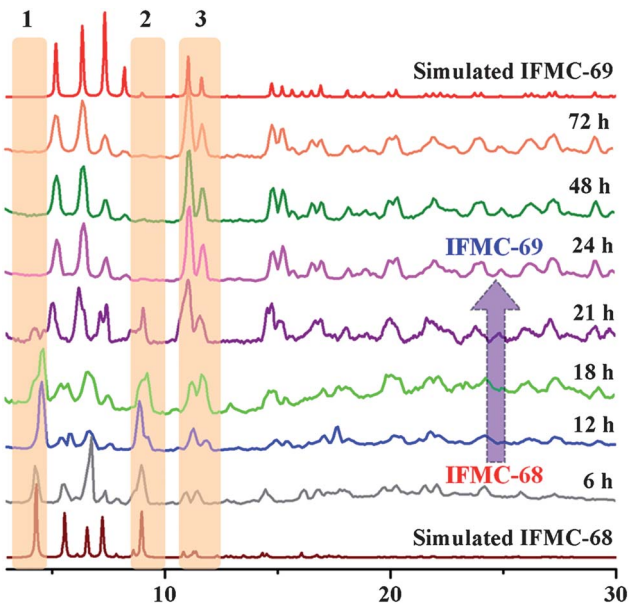

Fig. 4 Powder X-ray diffraction patterns of simulated IFMC-68 (dark red), IFMC-68 in a sealed Teflon reactor heated at 140 °C for 6 h (gray), 12 h (blue), 18 h (green), 21 h (purple), 24 h (pink), 48 h (dark green) and 72 h (orange), and simulated IFMC-69 (red).

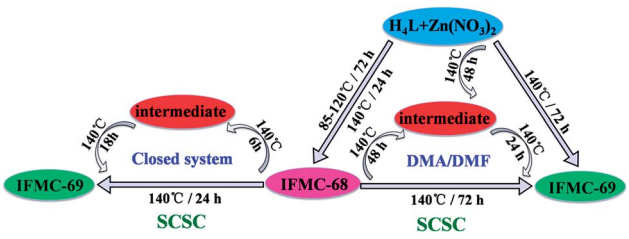

Scheme 1 The scheme of SCSC transformation between IFMC-68 and IFMC-69.

has been set at 438.15 K and the standard atmosphere pressure. The calculated results demonstrate the generation process of the $[Zn_4O(CO_2)_6]_2H_2O$ SBU is strongly exothermic, with enthalpy of −180.60 kcal mol^{-1}. As a result, this enthalpic contribution may drive the formation of the complex **IFMC-69**. Moreover, ΔrG is an important parameter in thermodynamic analysis, and the Gibbs free energy for this reaction shows that the formation of the $[Zn_4O(CO_2)_6]_2H_2O$ SBU is spontaneous with value of −51.94 kcal mol^{-1}. Therefore, it is clear from the theoretical simulations that the formation of **IFMC-69** is thermodynamically favorable.

Stability is one of the most crucial properties in the practical application for MOF materials.[16] Therefore the measurements of the stability based on **IFMC-68** and **IFMC-69** in air have also been conducted. When **IFMC-68** is exposed in air for 6 h, the framework is collapsed (Fig. S16†). Nevertheless **IFMC-69** can retain the integrity of the framework well after exposure in air for 2 months (Fig. S17†), presenting remarkable stability. Through the SCSC transformation we have achieved the conversion from an air-unstable MOF to an air-stable MOF.

The structure features of these two compounds encourage us to study the gas sorption properties of the evacuated frameworks. The samples were fully activated by the procedure described in ESI.† The PXRD results indicate that the integrity of **IFMC-69** was well maintained (Fig. S19†), but the framework of **IFMC-68** collapsed to some extent since some peaks of activated-**IFMC-68** weakened obviously (Fig. S18†). N_2 adsorption of **IFMC-68** and **IFMC-69** were carried out at 77 K (Fig. 5a). On the contrary to the porosity of these two compounds calculated by PLATON,[12] the high porosity crystal **IFMC-68** only has a N_2 adsorption amount of 4.50 cm^3 g^{-1}. This may be attributed to the collapse of the framework of **IFMC-68** after the removal of the solvent molecules, which is consistent with the PXRD results (Fig. S18†). All of these results (the stability of these two compounds) well agree with those from the theoretical calculations. **IFMC-69** displays typical Type-I sorption isotherm for microporous materials. The BET and Langmuir surface areas are 581.00 and 664.33 m^2 g^{-1}, respectively, and the pore volume of **IFMC-69** is 0.25 cm^3 g^{-1}. The adsorption amount of N_2 at saturation is approximately 165.9 cm^3 g^{-1}, which is equivalent to 71.4 N_2 per unit cell. Using the Horvath–Kawazoe (HK) method on the N_2 adsorption isotherms, the pore size distribution of **IFMC-69** shows its pore size is about 5.9 Å (Fig. S20†).

The H_2 adsorption amount of **IFMC-69** is 119.33 cm^3 g^{-1} (1.07 wt%) and 85.46 cm^3 g^{-1} (0.74 wt%) at 77 K and 87 K (Fig. S21†), which corresponds to 51.3 and 36.8 H_2 per unit cell, respectively. The H_2 adsorption enthalpy of **IFMC-69** is 6.63 kJ mol^{-1} at zero coverage, which is calculated from a variant of the Clausius–Clapeyron equation,[17] shown in Fig. S22b.†

We also study the possible application for **IFMC-69** on selective gas separation. As shown in Fig. 5b, the N_2 and CO_2 sorption isotherms were measured at 273 K and 298 K, respectively, and the adsorption data was listed in Table S2.† To our delight, the CO_2 uptake capacity is much higher than that of N_2. The calculated CO_2/N_2 adsorption selectivity is 32.7 : 1 at 298 K, and it is higher than those of zeolitic imidazolate frameworks (ZIFs) with colossal cages, ZIF-100 (25.0 ± 2.4 : 1) and ZIF-95 (18.0 ± 1.7 : 1),[18] which is regarded as excellent selective carbon dioxide reservoir. The CO_2/N_2 adsorption selectivity for **IFMC-69** is also better than that of our reported zeolite-like MOF (**IFMC-1**, 26.9 : 1 at 298 K).[19] In addition, the distinct difference of adsorption capacities between CO_2 and N_2 prompts us to survey the enthalpy of CO_2 adsorption. The CO_2 adsorption enthalpy of **IFMC-69** is 17.45 kJ mol^{-1} at zero coverage (Fig. S22a†). All the data reveals that **IFMC-69** shows the ability to absorb CO_2 selectively and may be used for potential materials to separate the CO_2/N_2 mixture.

The existing microporous pores of **IFMC-69** make it suitable as a host for absorbing small molecules.[20] When **IFMC-69** (100 mg) was immersed in a hexane solution of I_2 (3 mL, 0.01 mol L^{-1}) at room temperature, colorless **IFMC-69** gradually intensified to dark brown, and the dark purple solution faded in 2 h (Fig. S23a†). The entry of I_2 into the **IFMC-69** host framework leads to a distinct decrease of the emission intensity with the guest inclusion amount increasing (Fig. S26b†), which is ascribed to the host–guest photoinduced electron transfer (PET) effect.[21] TGA analyses (Fig. S29†) show that the encapsulated amount of I_2 is 29.48% and each unit cell in **IFMC-69** can accommodate about 15.86 I_2 molecules according to the molar ratios of I_2/Zn. **IFMC-68** can also adsorb I_2, however, the framework of **IFMC-68** partially collapsed as adsorbing I_2, just as shown in the picture (Fig. S30†). So we mainly study the

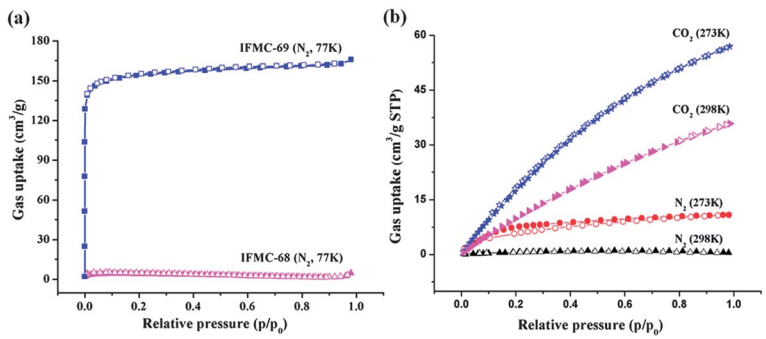

Fig. 5 (a) The N_2 gas–sorption isotherms for **IFMC-68** and **IFMC-69** at 77 K, 1 atm. (b) CO_2 and N_2 sorption isotherms of **IFMC-69** at different temperatures (blue: CO_2, 273 K; pink: CO_2, 298 K; red: N_2, 273 K; black: N_2, 298 K). The filled and open squares represent adsorption and desorption branches, respectively.

property of adsorbing I_2 for **IFMC-69**. When the crystals of **I_2@IFMC-69** were soaked in dry ethanol, the color of the crystals changed gradually from dark brown to light yellow in about 2.5 h and the colorless solution deepened into dark brown (Fig. S23b†). The release of I_2 resulted in the emission spectra intensity recovering by degrees (Fig. S26c†), the concentration of I_2 in ethanol increased with time. So the photographs and luminescent spectrum for **IFMC-69** releasing I_2 demonstrate that the I_2 sorption progress of **IFMC-69** is reversible. The tests of the electrical conductivity values (σ) of **I_2@IFMC-69** and **IFMC-69** were carried out. Notably, we get the electrical conductivity values (σ) of 2.80×10^{-6} S cm^{-1} for **I_2@IFMC-69** which is 2.24×10^7 times higher than **IFMC-69** (1.25×10^{-13} S cm^{-1}). When **IFMC-69** is adsorbing I_2, the potential intermolecular interactions between I_2 and π-electron walls are important, as they allow a single path for I_2 molecules to access and be restricted within well-regulated narrow limits within the channels, inducing $n \rightarrow \sigma^*$ charge transfer (CT).[22,23] Such an arrangement can result in cooperative electrical conductivity for **I_2@IFMC-69**. Therefore, **I_2@IFMC-69** could be used for potential semiconductor materials in the future.

Experimental

Synthesis of IFMC-68 ($[(Zn_4O)_2(L)_3]\cdot 10H_2O\cdot 46DMA$)

A solution of $Zn(NO_3)_2\cdot 6H_2O$ (0.150 g, 0.504 mmol) and H_4L (0.050 g, 0.081 mmol) in DMA (5 mL) was heated at 85 °C for 72 h in a Teflon-lined steel container. The resulting colorless crystals were collected, washed with Et_2O, and dried at room temperature (yield: 79% based on H_4L). Elemental microanalysis for $[(Zn_4O)_2(L)_3]\cdot 10H_2O\cdot 46DMA = C_{283}H_{506}O_{94}N_{46}Zn_8$, calculated (%): C, 51.68; H, 7.69; O, 22.87; N, 9.80; Zn, 7.96. Found (%): C, 51.36; H, 7.97; O, 23.15; N, 9.83; Zn, 7.69. IR (cm^{-1}): 3471.32 (m), 3071.25 (s), 2931.82 (m), 2545.31 (s), 1669.04 (w), 1604.60 (w), 1388.86 (w), 1302.23 (m), 1244.74 (w), 1172.24 (m), 1143.80 (s), 1096.23 (w), 1060.65 (m), 1016.97 (m), 785.46 (w), 635.26 (s), 544.47 (s), 406.85 (s).

Synthesis of IFMC-69 ($[(Zn_4O)_2(L)_3H_2O]\cdot H_2O\cdot 4DMA$)

A solution of $Zn(NO_3)_2\cdot 6H_2O$ (0.150 g, 0.504 mmol) and H_4L (0.050 g, 0.081 mmol) in DMA (5 mL) was heated at 140 °C for 72 h in a Teflon-lined steel container. The resulting colorless crystals were collected, washed with Et_2O, and dried at room temperature (yield: 63% based on H_4L). Elemental microanalysis for $[(Zn_4O)_2(L)_3H_2O]\cdot H_2O\cdot 4DMA = C_{115}H_{112}O_{44}N_4Zn_8$, calculated (%): C, 49.75; H, 4.03; O, 25.36; N, 2.02; Zn, 18.84. Found (%): C, 49.36; H, 4.29; O, 25.23; N, 2.46; Zn, 18.66. IR (cm^{-1}): 3438.95 (m), 2937.81 (w), 1667.23 (s), 1604.47 (s), 1559.61 (s), 1409.51 (s), 1304.52 (m), 1243.34 (s), 1170.22 (m), 1097.46 (w), 1030.91 (m), 925.29 (w), 856.92 (w), 782.54 (m), 694.89 (w), 660.21 (m), 474.79 (w).

The process of SCSC transformation

Method 1: 50 mg **IFMC-68** was sealed in a Teflon liner with 5 mL DMA and heated at 140 °C for 72 h, the colorless block single crystals of **IFMC-69** were collected.

Method 2: 50 mg **IFMC-68** was sealed in a Teflon liner without solvent and heated at 140 °C for 24 h, the colorless block single crystals of **IFMC-69** were collected.

Conclusions

In summary, we have reported here an interesting example of a solid-state SCSC transformation from an achiral MOF into a chiral MOF. To our knowledge, it is the first representative that the non-interpenetrated structure transforms into a self-penetrated structure in MOFs. There are the dimerization of Zn_4O clusters $[Zn_4O(CO_2)_6]_2H_2O$ in **IFMC-69**, and it represents the first example that the classic $Zn_4O(CO_2)_6$ SBU connected by water. More importantly, we have achieved the conversion from an air-unstable structure to an air-stable one, and the air-stable **IFMC-69** exhibits the selective CO_2 uptake over N_2 and more excellent gas adsorption ability than **IFMC-68**. We unprecedentedly study the influence of reaction temperature and time on SCSC transformation simultaneously, and then get the transformation relationship diagrams of **IFMC-68**, **IFMC-69** and the intermediate coming from the direct synthesis method and stepwise synthesis method based on different temperatures and time. Unusually, it is doubly triggered by reaction temperature and time simultaneously in either solvent or solid-state. I_2 adsorption experiments of **IFMC-69** exhibit a reversible process, and the electrical conductivity value (σ) of **I_2@IFMC-69** is much higher than that of **IFMC-69**. Therefore, **I_2@IFMC-69** can be used for potential semiconductor materials. Taking advantage of the above-mentioned study, the progress and mechanism of the SCSC transformation have been well understood, which can help us to learn more about the conversion nature of SCSC transformation and synthesize more SCSC materials in the future.

Acknowledgements

This work was financially supported by Pre-973 Program (2010CB635114), the National Natural Science Foundation of China (no. 21001020 and 21371099), the Jiangsu Specially-Appointed Professor, the Natural Science Research of Jiangsu Higher Education Institutions of China (no. 13KJB150021), the Priority Academic Program Development of Jiangsu Higher Education Institutions and the Foundation of Jiangsu Collaborative Innovation Center of Biomedical Functional Materials. We are thankful to Prof. Michael O'Keeffe for his kind structure analysis.

Notes and references

‡ Crystal data for **IFMC-68**: $C_{283}H_{506}O_{94}N_{46}Zn_8$, $M = 6576.33$, trigonal, space group $R\bar{3}c$, $a = 26.669(3)$, $c = 86.622(4)$ Å, $V = 53\,355(9)$ Å^3, $Z = 12$, $\mu = 0.554$ mm^{-1}, $D_c = 0.447$ Mg m^{-3}, $F(000) = 86\,379$, 10 440 unique ($R_{int} = 0.1222$), $R_1 = 0.1675$, w$R_2 = 0.0780$ ($I > 2\sigma(I)$), GOF = 0.700. Max/min residual electron density 0.234 and −0.177 e Å^{-3}. A total of 10 440 data were measured in the range $1.29 < \theta < 24.98°$. Crystal data for **IFMC-69**: $C_{115}H_{112}O_{44}N_4Zn_8$, $M = 2776.23$, cubic, space group $P23$, $a = 23.9647(14)$ Å, $V = 13\,763.1(14)$ Å^3, $Z = 12$, $\mu = 1.434$ mm^{-1}, $D_c = 1.163$ Mg m^{-3}, $F(000) = 70\,389$, 8180 unique ($R_{int} = 0.1134$), $R_1 = 0.1697$, w$R_2 =$

0.2683 ($I > 2\sigma(I)$), GOF = 0.913. Max/min residual electron density 0.711 and −0.600 e Å^{-3}. A total of 8180 data were measured in the range $1.20 < \theta < 25.11°$.

1 (*a*) Y.-C. He, J. Yang, G.-C. Yang, W.-Q. Kan and J.-F. Ma, *Chem. Commun.*, 2012, **48**, 7859; (*b*) Y.-J. Zhang, T. Liu, S. Kanegawa and O. Sato, *J. Am. Chem. Soc.*, 2009, **131**, 7942; (*c*) C.-H. Hu and U. Englert, *Angew. Chem., Int. Ed.*, 2005, **44**, 2281; (*d*) S. Kitagawa and K. Uemura, *Chem. Soc. Rev.*, 2005, **34**, 109; (*e*) T. Hoang, J.-W. Lauhe and F.-W. Fowler, *J. Am. Chem. Soc.*, 2002, **124**, 10656.

2 (*a*) H. Nakanishi, W. Jones, J.-M. Thomas, M.-B. Hursthouse and M. Motevalli, *J. Chem. Soc., Chem. Commun.*, 1980, 611; (*b*) C.-R. Theocharis and W. Jones, in *Organic Solid State Chemistry*, ed. G. R. Desiraju, Elsevier, 1987, ch. 2, p. 47.

3 (*a*) J. Sun, F.-N. Dai, W.-B. Yuan, W.-H. Bi, X.-L. Zhao, W.-M. Sun and D.-F. Sun, *Angew. Chem., Int. Ed.*, 2011, **50**, 7061; (*b*) J. Seo, R. Matsuda, H. Sakamoto, C. Bonneau and S. Kitagawa, *J. Am. Chem. Soc.*, 2009, **131**, 12792; (*c*) B. Li, R. J. Wei, J. Tao, R.-B. Huang, L.-S. Zheng and Z. Zheng, *J. Am. Chem. Soc.*, 2010, **132**, 1558; (*d*) R.-J. Wei, Q. Huo, J. Tao, R.-B. Huang and L.-S. Zheng, *Angew. Chem., Int. Ed.*, 2011, **50**, 8940; (*e*) L.-Q. Ma, C.-D. Wu, M.-M. Wanderley and W.-B. Lin, *Angew. Chem., Int. Ed.*, 2010, **49**, 8244.

4 M.-S. Chen, M. Chen, S. Takamizawa, T. Okamura, J. Fan and W.-Y. Sun, *Chem. Commun.*, 2011, **47**, 3787.

5 (*a*) M. Nihei, L.-Q. Han and H. Oshio, *J. Am. Chem. Soc.*, 2007, **129**, 5312; (*b*) M.-P. Suh, J.-W. Ko and H.-J. Choi, *J. Am. Chem. Soc.*, 2002, **124**, 10976.

6 (*a*) D. Liu, Z.-G. Ren, H.-X. Li, J.-P. Lang, N.-Y. Li and B.-F. Abrahams, *Angew. Chem., Int. Ed.*, 2010, **49**, 4767; (*b*) M.-H. Mir, L.-L. Koh, G.-K. Tan and J.-J. Vittal, *Angew. Chem., Int. Ed.*, 2010, **49**, 390; (*c*) N.-L. Toh, M. Nagarathinam and J.-J. Vittal, *Angew. Chem., Int. Ed.*, 2005, **44**, 2237; (*d*) Y.-C. Ou, D.-S. Zhi, W.-T. Liu, Z.-P. Ni and M.-L. Tong, *Chem.–Eur. J.*, 2012, **18**, 7357.

7 G.-C. Lv, P. Wang, Q. Liu, J. Fan, K. Chen and W.-Y. Sun, *Chem. Commun.*, 2012, **48**, 10249.

8 (*a*) Y.-Q. Lan, H.-L. Jiang, S.-L. Li and Q. Xu, *Inorg. Chem.*, 2012, **51**, 7484; (*b*) J. Tian, L.-V. Saraf, B. Schwenzer, S.-M. Taylor, E.-K. Brechin, J. Liu, S.-J. Dalgarno and P.-K. Thallapally, *J. Am. Chem. Soc.*, 2012, **134**, 9581.

9 (*a*) S.-B. Choi, H. Furukawa, H.-J. Nam, D.-Y. Jung, Y.-H. Jhon, A. Walton, D. Book, M. O'Keeffe, O.-M. Yaghi and J. Kim, *Angew. Chem., Int. Ed.*, 2012, **51**, 8791; (*b*) C.-L. Chen, A.-M. Goforth, M.-D. Smith, C.-Y. Su and H.-C. zur Loye, *Angew. Chem., Int. Ed.*, 2005, **44**, 6673; (*c*) D.-X. Xue, W.-X. Zhang, X.-M. Chen and H.-Z. Wang, *Chem. Commun.*, 2008, 1551.

10 (*a*) P.-B. Chatterjee, A. Audhya, S. Bhattacharya, S.-M.-T. Abtab, K. Bhattacharya and M. Chaudhury, *J. Am. Chem. Soc.*, 2010, **132**, 15842; (*b*) P. Zhu, W. Gu, L.-Z. Zhang, X. Liu, J.-L. Tian and S.-P. Yan, *Eur. J. Inorg. Chem.*, 2008, 2971; (*c*) T. Jacobs, J.-A. Gertenbach, D. Das and L.-J. Barbour, *Aust. J. Chem.*, 2010, **63**, 573; (*d*) C.-D. Wu and W. Lin, *Angew. Chem., Int. Ed.*, 2005, **44**, 1958; (*e*) Q.-K. Liu, J.-P. Ma and Y.-B. Dong, *J. Am. Chem. Soc.*, 2010, **132**, 7005.

11 (*a*) J.-Y. Lee, S.-Y. Lee, W. Sim, K.-M. Park, J. Kim and S.-S. Lee, *J. Am. Chem. Soc.*, 2008, **130**, 6902; (*b*) M.-H. Zeng, Q.-X. Wang, Y.-X. Tan, S. Hu, H.-X. Zhao, L.-S. Long and M. Kurmoo, *J. Am. Chem. Soc.*, 2010, **132**, 2561; (*c*) M.-C. Bernini, F. Gándara, M. Iglesias, N. Snejko, E.-G. Puebla, E.-V. Brusau, G.-E. Narda and M.-A. Monge, *Chem.–Eur. J.*, 2009, **15**, 4896; (*d*) X.-N. Cheng, W.-X. Zhang and X.-M. Chen, *J. Am. Chem. Soc.*, 2007, **129**, 15738.

12 A.-L. Spek, *J. Appl. Crystallogr.*, 2003, **36**, 7.

13 Y.-Q. Lan, H.-L. Jiang, S.-L. Li and Q. Xu, *Adv. Mater.*, 2011, **23**, 5015.

14 T.-F. Liu, J. Lu, X. Lin and R. Cao, *Chem. Commun.*, 2010, **46**, 8439.

15 (*a*) B.-J. Burnett, P.-M. Barron, C. Hu and W. Choe, *J. Am. Chem. Soc.*, 2011, **133**, 9984; (*b*) H.-J. Choi and M.-P. Suh, *J. Am. Chem. Soc.*, 2004, **126**, 15844.

16 Z. Yin, Q.-X. Wang and M.-H. Zeng, *J. Am. Chem. Soc.*, 2012, **134**, 4857.

17 S.-S. Kaye and J.-R. Long, *J. Am. Chem. Soc.*, 2005, **127**, 6506.

18 B. Wang, A.-P. Côté, H. Furukawa, M. O'Keeffe and O. M. Yaghi, *Nature.*, 2008, **453**, 207.

19 J.-S. Qin, D.-Y. Du, W.-L. Li, J.-P. Zhang, S.-L. Li, Z.-M. Su, X.-L. Wang, Q. Xu, K.-Z. Shao and Y.-Q. Lan, *Chem. Sci.*, 2012, **3**, 2114.

20 W.-W. He, S.-L. Li, G.-S. Yang, Y.-Q. Lan, Z.-M. Su and Q. Fu, *Chem. Commun.*, 2012, **48**, 10001.

21 B. Zhao, X.-Y. Chen, P. Liao, D.-Z. Cheng, S.-P. Yan and Z.-H. Jiang, *J. Am. Chem. Soc.*, 2004, **126**, 15394.

22 M.-H. Zeng, Q.-X. Wang, Y.-X. Tan, S. Hu, H. i.-X. Zhao, L.-S. Long and M. Kurmoo, *J. Am. Chem. Soc.*, 2010, **132**, 2561.

23 Z. Yin, Q.-X. Wang and M.-H. Zeng, *J. Am. Chem. Soc.*, 2012, **134**, 4857.